Prepared for submission to JHEP

UTTG-23-18
LCTP-18-24

arXiv:1811.05534v2 [hep-ph] 19 Nov 2018

Addressing Astrophysical and Cosmological Problems With Secretly Asymmetric Dark Matter

Christopher Dessert,[a] **Can Kilic,**[b] **Cynthia Trendafilova,**[b] **and Yuhsin Tsai**[c]

[a] *Leinweber Center for Theoretical Physics, Physics Department, University of Michigan, Ann Arbor, MI, 48109*

[b] *Theory Group, Department of Physics, The University of Texas at Austin, Austin, TX 78712*

[c] *Maryland Center for Fundamental Physics, University of Maryland, College Park MD 20742*

Abstract: We present a simple model of dark matter that can address astrophysical and cosmological puzzles across a wide range of scales. The model is an application of the Secretly Asymmetric Dark Matter mechanism, where several flavors of dark matter are fully asymmetric despite an exact dark matter number symmetry $U(1)_\chi$. The dark matter relic abundance arises from these asymmetries, generated in the early universe through right-handed neutrino decays. The $U(1)_\chi$ is gauged by a massless dark photon, and asymmetries with opposite signs in the different DM flavors result in the formation of bound states. Dark acoustic oscillations in the early universe lead to a suppression in the matter power spectrum for addressing the σ_8 problem. The dark photon as a relativistic degree of freedom contributes to ΔN_{eff}, easing the tension between the CMB and low redshift H_0 measurements. Finally, scattering between the bound states after structure formation leads to a flattening of the dark matter distribution at the cores of haloes.

Contents

1 Introduction **1**

2 The Model, and particle physics considerations **2**

3 Cosmology and astrophysical signatures **7**

3.1 Dark recombination(s) 8

3.2 Dark acoustic oscillations and large scale structure 10

3.3 Scattering between bound states and small scale structure 12

3.4 Reconciling the large and small scale structure problems 14

4 Conclusions **16**

1 Introduction

Secretly Asymmetric Dark Matter (SADM) has recently been proposed [1] as a mechanism to generate the dark matter (DM) relic abundance through an asymmetry in the dark sector despite an exact (global or gauged) DM number symmetry $U(1)_\chi$. In the implementation of this idea in ref. [1], the asymmetry is first generated in the visible sector through high-scale leptogenesis [2][1] and then transferred to a dark sector containing three DM flavors χ_i, a flavorless mediator ϕ, and a dark photon γ_D via a coupling to the right-handed leptons of the Standard Model (SM). The mediator in that case is charged both under SM hypercharge and under $U(1)_\chi$, and therefore leads to mixing between the photon and the dark photon at the one-loop level. This is phenomenologically only acceptable if the dark photon has a nonzero mass [5], and therefore the experimental signatures of the model manifest themselves at short distances, but in the context of long distance physics it falls under the collisionless cold DM category.

In this work we introduce a different implementation of the SADM mechanism, where a massless dark photon is phenomenologically allowed, and leads to a rich set of astrophysical signatures, despite the rather minimal high-energy setup. We argue that this setup is capable of addressing open questions in astrophysics both at the large (Hubble-scale) and small (galaxy-scale) scales simultaneously. The model we propose serves as a short-distance implementation of two mechanisms that have recently been proposed to address the same open questions, namely Dark Acoustic Oscillations [6–10] and Hidden Hydrogen DM [12, 13]. By focusing on a particular region of parameter space of the model, we show that the H_0 discrepancy [14], the σ_8 discrepancy [15–19] and the mass deficit problem [15, 20, 21] in dwarf galaxies and galaxy clusters can all be addressed. There have been many efforts in

[1] See reviews of leptogenesis such as ref.s [3, 4] for a comprehensive list of references.

the literature to address these discrepancies using non-standard DM self interactions [22–31]. The SADM model presented here extends these efforts by providing a minimal short-distance setup that nevertheless has rich enough dynamics to address multiple issues across a wide range of scales.

The core feature of the SADM mechanism is that due to the unbroken DM number symmetry, the total dark charge of the universe is zero at all times, but there can be several DM flavors that have individual asymmetries. Due to the crucial role of there being multiple DM flavors, SADM can be considered as a special case of the Flavored Dark Matter scenario [32–38]. Unlike the model studied in ref. [1] however, where the heavier DM flavors decay to the lightest one before Big Bang Nucleosynthesis (BBN) and result in a symmetric distribution of the lightest DM flavor at late times, in the model we study in this work all DM flavors are extremely long-lived and are still present today. This means that flavors with opposite signs of asymmetry (and with opposite dark charges) must coexist, along with a massless dark photon that mediates long-range interactions, and therefore multiple bound states can form, each one behaving as atomic DM [22, 39, 40]. These bound states, along with unbound DM particles and the massless dark photon then give rise to rich dynamics across a range of distance scales. The dark photon as an additional relativistic degree of freedom helps ease the tension between CMB-based [41] and low redshift [14, 42, 43] measurements of H_0, dark acoustic oscillations in the early universe that arise from the scattering of free and bound states leads to a suppression of the matter power spectrum at small scales, and the scattering between bound states after structure formation leads to a flattening of the DM density distribution inside haloes.

The layout of this paper is as follows: In section 2 we introduce the short-distance model, and we consider its phenomenology in the context of particle physics observables and constraints. In section 3 we then study the cosmological features of the model, and the astrophysical signatures that it gives rise to at the large and small scales. We conclude in section 4 and we consider directions for future research.

2 The Model, and particle physics considerations

In this section we will introduce our SADM model and consider its high energy aspects. We assume heavy right handed neutrinos N_i exist and that they have Majorana masses as well as a Yukawa coupling to the SM leptons

$$\mathcal{L} \supset M_{N,ij} N_i N_j + Y^N_{ij} N_i \ell_j H^\dagger + \text{h.c.}, \tag{2.1}$$

where H is the SM Higgs doublet. This well-studied extension of the SM generates both light neutrino masses through the see-saw mechanism and it also allows the creation of a net $B - L$ number as the origin of the matter-antimatter asymmetry in the SM sector through CP violating phases in the coupling matrix Y^N_{ij}. These features are explored in depth in reviews of leptogenesis [3, 4].

To this setup we add three flavors of Dirac fermions $(\chi, \chi^c)_i$ and a scalar ϕ with the couplings (in the χ-mass basis)

$$\mathcal{L} \supset M_\phi^2 |\phi|^2 + m_{\chi,i} \chi^c_i \chi_i + \lambda_{ij} N_i \chi_j \phi + \text{h.c.}. \tag{2.2}$$

The λ_{ij} coupling matrix contains physical phases and is a source of CP-violation in the dark sector. Purely for reasons of simplicity we choose the N to only couple to the left-handed χ but not the right-handed χ^c. A more general setup with both types of couplings and with independent coupling matrices λ_{ij} and $\tilde{\lambda}_{ij}$ is possible, and this would not significantly change the conclusions of our paper, as long as the couplings are still CP-violating. We will soon introduce a convention for assigning the flavor labels i. Note that an exact $U(1)_\chi$ symmetry exists, under which all χ have charge +1, while all χ^c and ϕ have charge -1. We will take this symmetry to be gauged by the dark photon, with a fine structure constant α_d.

The mediator ϕ, being a scalar, will be taken to be heavy, though we will assume that it is lighter than the right-handed neutrinos. Once the right-handed neutrinos become non-relativistic and the interaction of equation 2.2 drops out of equilibrium, the SM and dark sectors decouple from one another. As the heavy neutrinos N decay, they will then generate asymmetries both in the SM leptons and in the dark sector (in ϕ and the χ_i); however as mentioned before $U(1)_\chi$ is never broken and therefore the total dark charge of the universe is zero at all times. With the interaction of equation 2.2 out of equilibrium, the asymmetries generated in the three χ flavors cannot wash each other out. As the temperature drops further, the ϕ particles become nonrelativistic and the symmetric part of the ϕ particle distribution annihilates to dark photons. The asymmetric ϕ particles then decay as $\phi \to \chi\, \ell^\pm H^\mp$, transferring their dark charge to the χ flavors, such that after the ϕ decays the asymmetry in the dark sector will reside entirely in the three DM flavors, in such a way that the total dark charge of the universe remains zero. Note that the heaviness of both ϕ and N means that the χ are very challenging to access in collider, direct detection, or indirect detection experiments. Our model does however have astrophysical signatures, which are the focus of this paper and which we will study in the next section.

Assuming generic phases in the entries of the Y^N_{ij} and the λ_{ij} matrices, the ratio of the typical magnitudes of the elements of Y^N_{ij} and the typical magnitudes of the elements of λ_{ij} will determine the branching ratio of the decaying N into the visible vs the dark sector, and thereby the ratio of the overall lepton number (more precisely, $B-L$ number) and the flavor-by-flavor χ asymmetries that are generated through heavy neutrino decays.

Therefore, for similar magnitudes in the entries of the Y^N_{ij} and the λ_{ij} matrices, the fact that $\Omega_{DM} \sim 5\Omega_B$ suggests the GeV scale for the mass of the heaviest χ flavor, but if the entries of one coupling matrix are larger than those of the other, then this mass can also vary in either direction. As we will show in section 3, the region of parameter space that is of interest for us has the mass of the heaviest DM flavor $\sim \mathcal{O}(10)$ GeV, the mass of the lightest DM flavor $\sim \mathcal{O}(1)$ MeV, and a value for α_d of order several percent. In this parameter region, the symmetric parts of the χ distributions annihilate efficiently, leaving behind only the asymmetric part generated during the N decays.

The asymmetry generated in the different χ flavors will differ from one another. In fact, due to the total dark charge of the universe being zero, there will always be one χ flavor with one sign of the asymmetry, and two flavors with the opposite sign, after the ϕ particles have all decayed. We will adopt the following naming convention for the three χ flavors: The χ flavor which is unique in its sign of the asymmetry will be labeled χ_1, whereas the

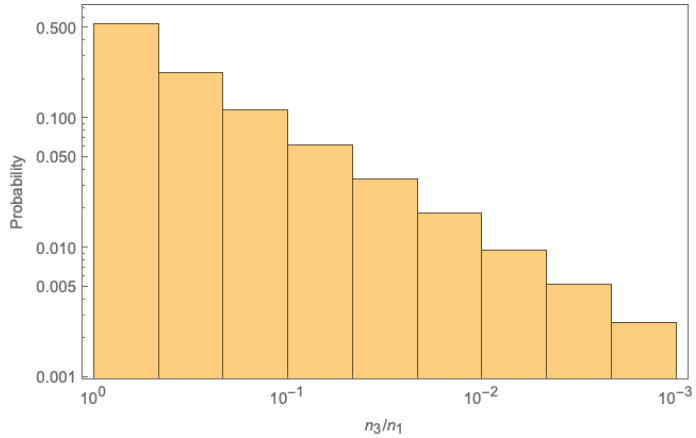

Figure 1. The estimate of the probability distribution function for the ratio n_3/n_1. See main text for the details of the calculation.

two χ flavors with the other sign of the asymmetry will be labeled χ_2 and χ_3, such that $m_{\chi_2} > m_{\chi_3}$. As we will see in the next section, the most interesting phenomenology is obtained when χ_3 and not χ_1 is the lightest DM flavor. Thus we will take $m_{\chi_1} > m_{\chi_3}$ as well, while either one of χ_1 or χ_2 could be the heaviest flavor. The possible bound states are then formed between χ_1 and χ_2, labeled H_{12}, and between χ_1 and χ_3, labeled H_{13}. Since the total dark charge of the universe is zero at all times, the asymmetries of χ_2 and χ_3 add up in magnitude to that of χ_1.

The overall size of the entries of the λ_{ij} coupling matrix determines the branching fraction of N to the dark sector, and therefore the overall size of the asymmetries of all χ flavors, while the specific flavor and phase structure in the coupling matrix determines the branching fractions among the DM flavors. The three comoving asymmetries ΔY_i of the χ flavors (after ϕ decays) satisfy $\sum_{i=1}^{3} \Delta Y_i = 0$. In terms of the physical number densities of the three χ particles (or antiparticles, depending on the sign of the asymmetry), this can also be written as $n_1 = n_2 + n_3$. Thus the n_i are not independent, however the ratio n_3/n_1 can in principle have any value in the interval $[0, 1]$.

We can estimate the probability distribution for this ratio using Monte Carlo methods with a prior where each entry of the 3×3 matrix λ_{ij} is randomly chosen over the unit complex circle. To calculate the asymmetry generated in each flavor from a given matrix λ_{ij}, we follow standard techniques from leptogenesis [3]. We assume the heavy neutrino masses are hierarchical with $m_{N_1} \ll m_{N_2}, m_{N_3}$ (we use $m_{N_1} = 1.0 \times 10^{16}$ GeV as a benchmark value). N_1 decays are fast compared to the Hubble scale, and therefore the asymmetry production takes place in the strong washout regime. Ratios of the ΔY_i generated in the N_1 decays can be obtained form the ratios of the CP asymmetry factors for each flavor i

$$\epsilon_{ii} \propto \mathrm{Im}\{[\lambda]_{1i}[m^*\lambda]_{1i}\}, \tag{2.3}$$

where the matrix $[m]_{ij}$ is given by

$$[m]_{ij} = [\lambda]_{ki}[\lambda]_{kj}/m_{N_k}. \tag{2.4}$$

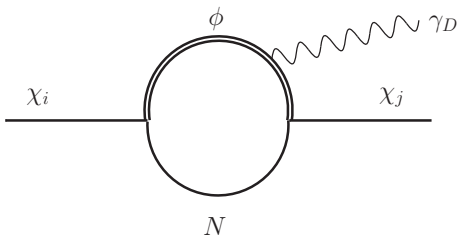

Figure 2. Decay mode for a heavier DM flavor to decay to a lighter one.

For the branching ratios of the subsequent ϕ decays, only the tree level contributions with an off-shell N_1 are used, since any additional CP violation introduced at this stage is subdominant. Note also that an *overall* rescaling of all λ_{ij} entries does not affect the probability distribution of n_3/n_1, and therefore we are not committing ourselves to a particular size of the λ_{ij} couplings by generating random numbers over the complex unit circle. For a given choice of m_{N_1} and m_{χ_i}, such a rescaling can be chosen such that the correct overall ρ_{DM} and ρ_B are obtained. The result for the n_3/n_1 probability distribution is shown in figure 1. As we will see in the next section, the region of greatest phenomenological interest corresponds to $n_3/n_1 \lesssim 0.1$, which does not require significant fine-tuning.

Even without a compressed spectrum among the DM flavors, all χ are extremely long-lived, and are still undecayed today. The leading decay mode arises from the one-loop diagram shown in figure 2. After integrating out N and ϕ, this diagram gives rise to a flavor off-diagonal dipole term for χ at low energies, the coefficient of which can be estimated as (we use λ to stand in for any $\mathcal{O}(1)$ entries in the λ_{ij} coupling matrix):

$$\Gamma \approx \frac{1}{8\pi}\left(\frac{\lambda^2}{m_N}\frac{e_D}{16\pi^2 m_\phi^2}\right)^2 m_\chi^7 \tag{2.5}$$

$$= (10^{-47}\text{eV})\left(\lambda^4 e_D^2\right)\left(\frac{m_\chi}{100\text{GeV}}\right)^7\left(\frac{10^{12}\text{GeV}}{m_N}\right)^2\left(\frac{10^{10}\text{GeV}}{m_\phi}\right)^4 \tag{2.6}$$

$$\ll H_0 \approx 10^{-33}\ \text{eV}. \tag{2.7}$$

The lifetime is many orders of magnitude larger than the age of the universe for the parameter region that will be used in this paper. The leading tree-level decay diagrams are even further suppressed than this decay mode, and are therefore irrelevant.

As we will see in the next section, the most interesting phenomenological features of the model will be obtained when the mass of the heaviest flavor (χ_1 or χ_2) is $\mathcal{O}(10)$ GeV, the mass of the next heaviest flavor is $\mathcal{O}(0.1-1)$ GeV, and the mass of the lightest flavor (χ_3) is $\mathcal{O}(1)$ MeV. This means that H_{12} will be strongly bound and difficult to ionize, serving as a neutral DM component, while H_{13} may be easy to ionize, such that a non-negligible fraction of χ_3 (and the corresponding amount of χ_1) can be unbound at certain times during the early universe, delaying the decoupling of the dominant DM component from the dark radiation, and leading to interesting dynamical effects.

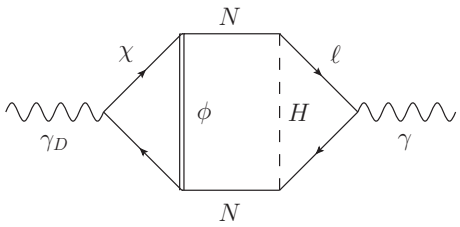

Figure 3. Leading contribution to mixing between the dark photon and the SM photon.

For a massless dark photon, it needs to be checked that the mixing with the SM photon is acceptably small. More precisely, in the basis where γ_D only interacts with χ but not the SM fermions, the millicharge acquired by χ under electromagnetism needs to be small. The γ-γ_D mixing is induced at the three-loop level: see figure 3. Matching on to an effective operator $\epsilon F_D^{\mu\nu} F_{\mu\nu}$, one can estimate

$$\epsilon \sim \frac{e e_D \lambda^2 Y^2}{(16\pi^2)^3}. \tag{2.8}$$

If $\lambda^2 \sim Y^2 \sim 0.1$ and $\alpha_d \sim \alpha$, then ϵ is below 10^{-10}. Let us compare this to the constraints for millicharged DM (figure 1 in ref. [44], with $m \sim \mathcal{O}(10)$ GeV, the mass of the heaviest DM flavor), keeping in mind that some of the constraints will be relaxed, as these were derived with the assumption that all DM particles are millicharged while we will focus in this work exclusively on the possibility that all but a small fraction of the χ particles are in bound states, and therefore have no *net* millicharge. In particular, the leading constraints from galactic and cluster magnetic fields probe the DM at small momenta, or at distance scales larger than the size of the bound states, thus these constraints cannot resolve the millicharges of the constituents. While the momentum scale that is probed at LUX is still too small to resolve the constituents of H_{12}, it may be sufficiently large to resolve the constituents of H_{13}. However, in the parameter space of interest to us, H_{13} is the subdominant DM component, which relaxes the constraints below the generic values of ϵ in our model. Furthermore, for a significant fraction of the parameter region of interest to us (especially when $m_{\chi_2} > m_{\chi_1}$), the mass of H_{13} is below the sensitivity of LUX. It is however interesting to note that future direct detection experiments with a low mass threshold may be able to test the scenario presented here. Finally, for the parameter region of interest, the value of ϵ in our model is also below the bounds from supernovae [5].

As a final consideration about the particle physics nature of our model, we want to address the potential concern that flavor oscillations between the DM flavors may cause a washout of the asymmetries, as the particles of χ_1 oscillate into the antiparticles of χ_2 or χ_3, or the other way around. However, the large mass gap between the χ flavors in the parameter region of interest in this paper, and the extremely small intrinsic widths of these states makes oscillations so small that they are negligible for all intents and purposes.

3 Cosmology and astrophysical signatures

Having discussed the short-distance physics aspects of our model, we now turn our attention to the role it plays in the dynamics of the early universe, as well as in late-time astrophysical processes. Although the dark sector is hidden from direct experimental probes via non-gravitational interactions, the dynamics within the SADM sector can significantly change the gravitational potential in the early universe and it leaves visible signals on both the large and small scale structures. We will show that there is a region of parameter space where observational anomalies on scales of dwarf galaxies ($\sim$ kpc size) [15, 20], galaxy clusters ($\sim$ Mpc size) [21], the σ_8 problem ($\sim$ 10 Mpc size) [15–19], and the tension in the measurements of H_0 from the CMB [41] and from low redshift measurements [45] may all be addressed.

The input parameters of the model that are relevant at large distances can be listed as the comoving asymmetries of the χ flavors (of which only two are independent, and which can therefore be parameterized in terms of n_1 and n_3/n_1 once the symmetric part of the χ distributions annihilates away), the masses of the three χ flavors, and α_d. In order to calculate how the temperature of the dark sector is related to that of the SM sector, consider energies above m_N where the interaction of equation 2.2 keeps the two sectors in equilibrium. As the temperature drops below m_N, the visible and dark sectors decouple. At this time, the dark sector contains the three Dirac fermions $\chi_{1,2,3}$, the complex scalar ϕ, and the dark photon γ_D. ϕ is only somewhat lighter than the N, and for the parameter region of interest for us, the mass of the lightest flavor is $\mathcal{O}(1)$ MeV. Therefore, at the time of structure formation, only γ_D is still relativistic.

If there are no other degrees of freedom in the visible sector other than those of the SM up to energies of m_N, then by using the ratio of the number of relativistic degrees of freedom in the two sectors at the decoupling scale and at the scale of structure formation, one obtains $\Delta N_{eff} = 0.75$. However, since the two sectors decouple at a very high temperature scale, one needs to take into account the possibility that the visible sector contains additional degrees of freedom (e.g. connected to the solution of the electroweak naturalness problem, grand unification, etc.) that release additional entropy in the visible sector as the universe cools down, and thereby further suppress ΔN_{eff}. The value 0.75 should therefore be considered as an upper limit, with the actual value depending on other possible extensions of the SM. Since a value of 0.75 is outside the 2σ contour for reconciling the H_0 discrepancy (see e.g., [41]), we will adopt a benchmark value of $\Delta N_{eff} = 0.60$ for the remainder of the paper[2], which can be obtained for example if there are six Dirac fermions beyond the SM in the visible sector. Adding even more degrees of freedom to the visible sector would further reduce ΔN_{eff}. It should also be noted that at the time of BBN, ΔN_{eff} is even smaller ($\Delta N_{eff} = 0.42$) since χ_3 has not yet become nonrelativistic at that time for $m_{\chi_3} \lesssim$ MeV, which is the preferred value for addressing the σ_8 problem as we will see later. Thus our model is compatible with BBN constraints [47].

[2] According to Fig. 35 in [41], this rather large ΔN_{eff} is within 2σ constraint from the joint Planck TT,TE,EE+lowE+lensing+BAO fit including the low redshift measurement [46].

There are two recombination processes during the early universe, of χ_1 with χ_2 into H_{12}, and of the remaining χ_1 with χ_3 into H_{13}. H_{12} forms earlier due to its larger binding energy, and the remaining χ_1 and χ_3 particles scatter with each other and remain in thermal equilibrium at this time. Similar to the proton-hydrogen scattering in the SM sector, the scattering cross section between the non-relativistic χ_1 and the H_{12} bound state is larger than the geometrical size of H_{12} [48], sufficient for keeping them in thermal equilibrium with each other. While χ_1-χ_3 scattering is also efficient, the entire dark sector is then in thermal equilibrium with the dark photon, and the resulting DM oscillations delay the formation of large scale structure. The oscillation stops as H_{13} recombines, which leaves too few free (dark-)charged particles to sustain the oscillations. These dark acoustic oscillations generate a small but visible damping of the matter power spectrum and may provide a solution to the σ_8 problem. A more complete parameter fitting procedure including also the CMB and BAO data is necessary to confirm this claim in full detail, however in this work we will take a simpler approach and we will calculate the size of power spectrum suppression to argue that the claim is plausible, leaving a more detailed analysis to future work.

We will also show that at later times, during the formation of DM halos, the scattering between H_{12} bound states leads to thermal equilibrium and provides a solution to the core/cusp problem of dwarf galaxies. The non-trivial velocity dependence due to the inelastic scattering $H_{12}H_{12} \to H_{12}H_{12}\,\gamma_D$ through the dark hyperfine transition also gives the right cross section for cores to form in relaxed cluster halos. As we will see, achieving this will favor the parameter region where the heaviest DM flavor mass is $\sim \mathcal{O}(10)$ GeV, where the value of α_d is a few percent, and $n_3/n_1 \sim 0.1$. Furthermore, we will see that achieving the correct amount of damping of large scale structure favors the MeV range for m_{χ_3}. Thus there is a region of the parameter space of our model where all parameters are technically natural and where all three structure formation problems (dwarf, cluster and σ_8) and the H_0 tension could be addressed. Below, we explore each of these aspects of our model in detail.

3.1 Dark recombination(s)

The formation of the H_{12} and H_{13} bound states plays an important role in structure formation. In particular dark acoustic oscillations end when there are no longer sufficiently many unbound χ particles left to sustain them. Similar to the recombination of hydrogen in the SM, for both H_{12} and H_{13}, recombination proceeds through the formation of the excited states ($n \geq 2$), with a subsequent decay into the ground state either through a two photon emission or through a Lyman-α transition, where the dark photon becomes redshifted before ionizing other bound states.

A brief note on notation: we have introduced n_i in the previous section to denote the physical densities in each flavor. Since in this section we will also need to keep track of just the density of unbound particles in each flavor, we will introduce the notation n_i^f, where f stands for "free". With this definition $n_1 = n_1^f + n_{H_{12}} + n_{H_{13}}$, $n_2 = n_2^f + n_{H_{12}}$ and $n_3 = n_3^f + n_{H_{13}}$. We also define the ionization fraction in each flavor as $X_i \equiv n_i^f/n_i$.

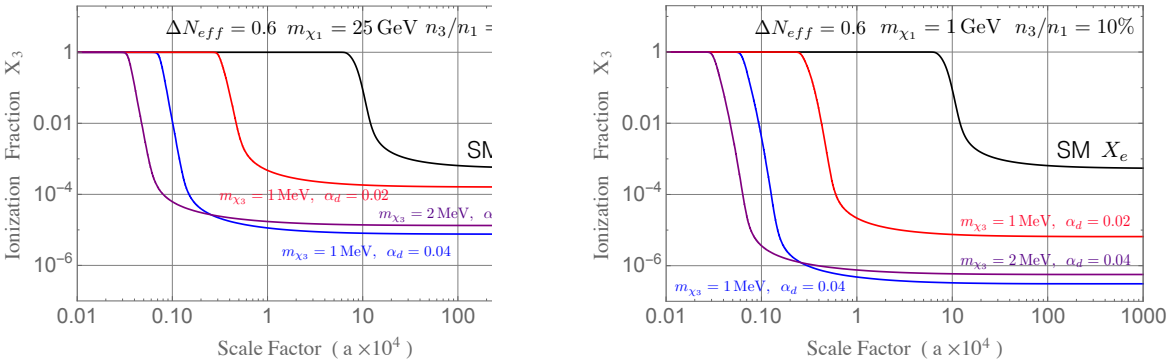

Figure 4. The SM (black) and χ_3 ionization fractions during the recombination epoch as a function of the scale factor, for representative values of (m_{χ_3}, α_d) and two χ_1 masses corresponding to the cases where χ_1 is the heaviest DM flavor (left), and the second heaviest DM flavor (right).

Note that the dark charge neutrality of the universe enforces both $n_1 = n_2 + n_3$ and also $n_1^f = n_2^f + n_3^f$.

The Boltzmann equation for $X_{2,3}$, can be written as [13]

$$\frac{dX_{2,3}}{dt} = C_{2,3}\Big\{(1 - X_{2,3})\beta_{2,3} - X_{2,3}\, n_1^f \alpha_{2,3}^{(2)}\Big\}, \quad \beta_{2,3} \equiv \alpha_{2,3}^{(2)} \left(\frac{m_{2,3}\, T_d}{2\pi}\right)^{3/2} e^{-\epsilon_{2,3}/T_d}. \quad (3.1)$$

Here, T_d stands for the temperature of the dark photon bath, and $\epsilon_{2,3}$ stands for the binding energy of H_{12} and H_{13}, respectively, given by $\mu\, \alpha_d^2/2$, with μ the reduced mass of the bound state in question. $\beta_{2,3}$ is the recombination rate, which relates to the ionization rate of the excited $(n = 2)$ state

$$\alpha_{2,3}^{(2)} = 9.78 \frac{\alpha_d^2}{m_{\chi_{2,3}}^2} \left(\frac{\epsilon_{2,3}}{T_d}\right)^{1/2} \ln\left(\frac{\epsilon_{2,3}}{T_d}\right). \quad (3.2)$$

The factor $C_{2,3}$ takes into account Peebles' correction to the process, and its value can be approximated as

$$C_{2,3} = \frac{\Lambda_{\alpha(2,3)} + \Lambda_{2\gamma_D(2,3)}}{\Lambda_{\alpha(2,3)} + \Lambda_{2\gamma_D(2,3)} + \beta_{2,3}^{(2)}}, \quad \Lambda_{\alpha(2,3)} = \frac{H(3\,\epsilon_{2,3})^3}{(8\pi)^2 n_{2,3}(1 - X_{2,3})}, \quad (3.3)$$

with H being the Hubble rate. $\Lambda_{2\gamma_D(2,3)}$ stands for the two photon decay rates of H_{12} and H_{13}, which we estimate by rescaling the SM result $\Lambda_{2\gamma} = 8.227$ sec^{-1} by the ratio of the relevant binding energies. The Lyman alpha production rate is $\beta_{2,3}^{(2)} = \beta_{2,3}\, e^{3\epsilon_{2,3}/4T_d}$. When calculating the ionization fractions, we calculate the Hubble expansion rate, keeping in mind that the dark and visible sectors have different temperatures, using the benchmark value $\Delta N_{eff} = 0.60$ as discussed above.

In Fig. 4, we plot X_3 during H_{13} recombination, for a few representative values of m_{χ_3} and α_d, for $n_3/n_1 = 10\%$. The plots on the left and right correspond to the case where χ_1 is the heaviest flavor with $m_{\chi_1} = 25$ GeV, and the case where it is the second heaviest flavor with $m_{\chi_1} = 1$ GeV, respectively. The relic ionization fraction becomes larger either

for a smaller value of α_d or a larger value of m_{χ_3}. The residual ionization fraction can be approximated as [10]

$$X_3 \sim 3 \times 10^{-6} \left(\frac{T_d}{T_\gamma}\right) \left(\frac{\alpha_d}{0.02}\right)^{-6} \left(\frac{n_1}{n_3}\right) \left(\frac{m_{H_{13}}}{\text{GeV}}\right) \left(\frac{\epsilon_3}{\text{keV}}\right). \tag{3.4}$$

Dark baryon acoustic oscillations end after H_{13} recombination, and the recombination time scale determines the suppression of the power spectrum. Since the H_{12} recombination happens at a much earlier time, it does not have a strong effect on the power spectrum.

3.2 Dark acoustic oscillations and large scale structure

We now turn our attention to the evolution equations for the DM and dark radiation (DR) density perturbations in our model, after the H_{12} recombination, but before the H_{13} recombination. Thus the relevant matter degrees of freedom are χ_1 (with $X_1 \sim n_3/n_1$ during this epoch), χ_3 (with $X_3 \sim 1$) and the bound state H_{12} (with $n_{H_{12}} \sim n_2$). Below, we will refer to these degrees of freedom collectively as "Acoustic DM" (AcDM) that undergo acoustic oscillations. We work in the conformal Newtonian gauge [49]

$$ds^2 = a^2(\tau)\left[-(1+2\psi)d\tau^2 + (1-2\phi)\delta_{ij}dx^i dx^j\right], \tag{3.5}$$

where the fields ψ and ϕ describe scalar perturbations on the background metric. To linear order in the perturbations, we have

$$\dot{\delta}_{\text{AcDM}} = -\theta_{\text{AcDM}} + 3\dot{\phi}\,, \tag{3.6}$$

$$\dot{\theta}_{\text{AcDM}} = -\frac{\dot{a}}{a}\theta_{\text{AcDM}} + \frac{4\rho_{\gamma_D}}{3\rho_{\text{AcDM}}} n_3^f(a)\sigma_T\, a(\theta_{\gamma_D} - \theta_{\text{AcDM}}) + k^2\psi, \tag{3.7}$$

where the derivatives are with respect to η, the conformal time. $\delta \equiv \delta\rho/\bar{\rho}$ is the perturbation of the energy density, k is the wave number, and $\theta \equiv \partial_i v^i$ is the divergence of the comoving 3-velocity. Since the AcDM components are all non-relativistic at this time, one can ignore the sound speed[3]. We consider the parameter region ($\alpha_d > 0.02$, $m_{\chi_3} < 10$ MeV), where all AcDM components remain coupled during the dark acoustic oscillations. As long as the momentum transfer rate from the dark Thomson scattering $\gamma_D\chi_3 \to \gamma_D\chi_3$ is comparable to Hubble, the density perturbations oscillate with the dark photon perturbation, and structures cannot grow. The cross section is given by $\sigma_T = 8\pi\alpha_d^2/3m_{\chi_3}^2$, and n_3^f depends on the ionization fraction X_3 obtained by solving Eq. (3.1). The dark photon perturbations, including higher modes in the Legendre polynomials, $F_{\gamma_D\ell}$, evolve as [49]

$$\dot{\delta}_{\gamma_D} = -\frac{4}{3}\theta_{\gamma_D} + 4\dot{\phi}, \tag{3.8}$$

$$\dot{\theta}_{\gamma_D} = k^2\left(\frac{1}{4}\delta_{\gamma_D} - \frac{1}{2}F_{\gamma_D 2}\right) + a\, n_3^f\, \sigma_T(\theta_{\text{AcDM}} - \theta_{\gamma_D}) + k^2\psi, \tag{3.9}$$

$$\dot{F}_{\gamma_D 2} = \frac{8}{15}\theta_{\gamma_D} - \frac{3}{5}kF_{\gamma_D 3} - \frac{9}{10}a\, n_3^f\, \sigma_T F_{\gamma_D 2}, \tag{3.10}$$

$$\dot{F}_{\gamma_D l} = \frac{k}{2l+1}\left[lF_{\gamma_D(l-1)} - (l+1)F_{\gamma_D(l+1)}\right] - a\, n_3^f\, \sigma_T F_{\gamma_D l}, \quad l \geq 3 \tag{3.11}$$

[3] We have verified numerically that this gives a good approximation.

$$\dot{F}_{\gamma_D l_{\max}} = k F_{\gamma_D (l_{\max}-1)} - \frac{l_{\max}+1}{\tau} F_{\gamma_D l_{\max}} - a\, n_3^f\, \sigma_T F_{\gamma_D l_{\max}}. \tag{3.12}$$

Here the $F_{\gamma_D l}$ are related to the spatial variations in the density fluctuations in the dark photons, in particular $\delta_{\gamma_D} \equiv F_{\gamma_D 0}$, $\theta_{\gamma_D} \equiv \frac{3}{4} k F_{\gamma_D 1}/4$, and $\sigma \equiv \frac{1}{2} F_{\gamma_D 2}$ where σ is the shear stress. We truncate the Boltzmann hierarchy at order $l_{\max} = 4$, making use of the approximation outlined in Ref. [49][4]. The equations are similar to those for the SM photon and baryons.

In the calculation we take $\psi = \phi$ and ignore the correction from free streaming radiation. This approximation is good since our ΔN_{eff} is much smaller than the number of light neutrinos. Gravity perturbations are sourced by the density fluctuations as described by the Einstein equation,

$$k^2 \psi + 3 \frac{\dot{a}}{a} \left(\dot{\psi} + \frac{\dot{a}}{a} \psi \right) = -\frac{a^2}{2 M_{pl}^2} \sum \rho_i\, \delta_i, \tag{3.13}$$

where the sum is over the SM photon, the dark photon and the AcDM components. For the initial conditions, the modes that enter the horizon before matter-radiation equality satisfy

$$\delta_{\gamma_D} = \frac{4}{3} \delta_{\rm AcDM} = -2\psi, \quad \theta_{\gamma,\gamma_D,{\rm AcDM}} = \frac{k^2 \eta}{2} \psi, \tag{3.14}$$

and the modes that enter during the era of matter domination satisfy

$$\frac{3}{4} \delta_{\gamma_D} = \delta_{\rm AcDM} = -2\psi, \quad \theta_{\gamma,\gamma_D,{\rm AcDM}} = \frac{k^2 \eta}{3} \psi. \tag{3.15}$$

We set the initial values of the higher modes $F_{\gamma_D \ell \geq 2} = 0$, since these higher angular modes quickly damp away when the AcDM-γ_D scattering is efficient. We neglect the tilt in the primordial spectrum ($n_s = 1$) and take a k-independent value of $\psi = 10^{-4}$. The final results are independent of the precise value of ψ since we are interested in the ratio of the matter power spectra with and without the dark acoustic oscillations. In the numerical study, we choose the values $h = 0.67$, $\Omega_\gamma h^2 = 2.47 \times 10^{-5}$, $\Omega_\Lambda h^2 = 0.69$, $\Omega_b h^2 = 2.2 \times 10^{-2}$, and $\Omega_\nu = 0.69 \Omega_\gamma$ [41].

After solving this set of differential equations, in order to quantify the importance of dark acoustic oscillations, we compare the DM power spectrum of AcDM to that of collisionless DM with an added non-interacting dark photon component, such that the energy density of dark radiation is equal in both scenarios, and further complications in the fitting of cosmological parameters are avoided:

$$\frac{P(k)_{\rm AcDM}}{P(k)_{\Lambda{\rm CDM+DR}}} \approx \left(\frac{\delta_\chi(k)_{\rm AcDM}}{\delta_\chi(k)_{\Lambda{\rm CDM+DR}}} \right)^2, \tag{3.16}$$

where the terms on the right hand side refer only to the nonrelativistic DM component. We show the power spectrum ratio in Fig. 5 for two representative values of α_d in the region of interest. When the H_{13} recombination takes place, the momentum transfer term in

[4] We have also reproduced the analysis with $l_{\max} = 5$ to confirm that our results are not sensitive to the choice of $l_{\max}$.

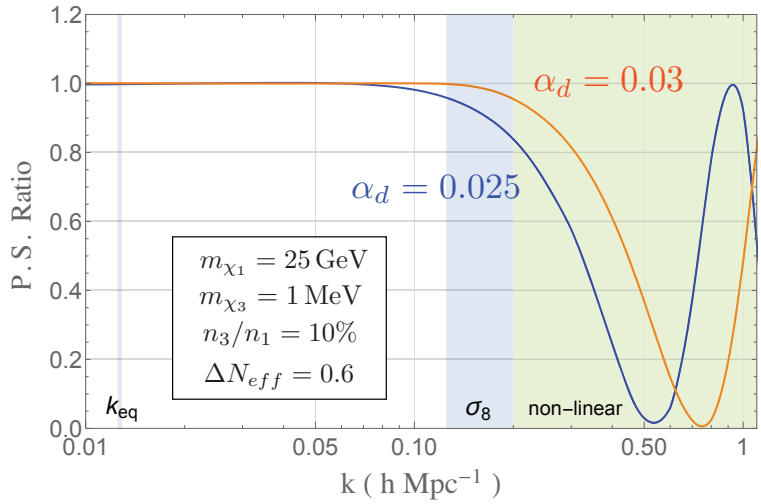

Figure 5. Ratio of the matter power spectrum between scenarios with and without dark acoustic oscillations, as is defined in Eq. (3.16). We use two representative values of α_d in the region of interest. The result is obtained by solving the linear order equations listed in the text. The ratio at large k is expected to receive further corrections from non-linear effects.

Eq. (3.7) quickly drops blow the Hubble expansion rate. The density perturbations entering the horizon after this point evolve the same way as they would in the ΛCDM scenario, and thus the ratio for small k modes asymptotes to 1. The matter power spectrum receives a suppression for modes that enter the horizon before recombination, thus for a lower H_{13} binding energy (blue curve) there is a larger suppression. This helps to explain the results of low red-shift measurements for σ_8. We estimate the viable parameter region by requiring a $5-15\%$ suppression of the power spectrum at $k = 0.2\,h$ Mpc^{-1} (blue band in figure 5 and yellow band in figure 6). Although in this work we only focus on the suppression of the matter power spectrum in the linear regime, the suppression continues past $k = 0.2h$ Mpc^{-1}. Once the non-linear corrections to the density perturbation are included, the galaxy survey data and Lyman-α observations, which probe the matter power spectrum at even larger k-modes, can be used to further constrain dark acoustic oscillations [11, 50–52], and thereby the parameter space of our model.

3.3 Scattering between bound states and small scale structure

After halo formation, the scattering cross section between the non-relativistic H_{12} bound states in the halo is roughly geometric in size, $\sigma \sim (\mu_{12}\alpha_d)^{-1}$. For the region of parameter space we are interested in, where the heaviest DM flavor has a mass of $\mathcal{O}(10)$ GeV and $\alpha_d \sim 10^{-2}$, the resulting cross section over mass ratio $\sigma/m_{H_{12}} \sim 0.1$ cm^2/g can be large enough to thermalize the bound states and change the DM density in the inner part of the halo. It was pointed out in Ref. [12] that dark hydrogen with a similar range of mass and couplings can explain the low DM density cores observed in small galaxies. Moreover, if

the hyperfine splitting of the bound state

$$E_{hf} = \frac{8}{3}\,\alpha_d^2\, f(R)^{-1} E_0, \quad R \equiv \frac{m_{\chi_1}}{m_{\chi_2}}, \quad f(R) = R + 2 + R^{-1} - \frac{\alpha_d^2}{2} \tag{3.17}$$

normalized by the energy scale $E_0 = \alpha_d^2\, \mu_{12}$ is comparable to the kinetic energy of the bound state, the effect of the inelastic hyperfine upscattering is to enhance the cross section of H_{12} self-interactions. The velocity dependence in this process makes the self-interaction cross sections in dwarf halos larger than that in cluster halos, giving the correct σ/m ratio to solve the mass deficit problem in galaxy clusters.

In order to show that the same mechanism also works in the region of parameter space that is of interest to us, we adopt the best fit value from ref. [12]

$$E_{hf} = 10^{-4} E_0 \tag{3.18}$$

and we limit ourselves to the range of α_d in Fig. 3 of [12], where both the dwarf and cluster data can be explained. Since we want the H_{12} self-interaction to solve the small scale structure problem, we choose $n_3/n_1 = 0.1$ as our benchmark value such that H_{12} and not H_{13} is the dominant component of DM, while the n_3 number density is not unnaturally small (see figure 1), and also not too small to maintain the thermal equilibrium in the early universe that is responsible for suppressing structure formation and addressing the σ_8 discrepancy.

Even though it constitutes a smaller fraction of the DM energy density, we need to assess whether the H_{13} bound state may still play a role in halo formation. In particular, the H_{13} bound state has a much larger radius than H_{12} due to the smallness of m_{χ_3}, and therefore scattering with H_{13} could potentially change the desired core size of the H_{12} halo. However, we find that this is not the case. For the parameter range we consider, the inverse Bohr radius of H_{13} (~ 10 keV) is still too small compared to to the value that would result in sufficient momentum transfer for keeping H_{12} atoms in thermal equilibrium both at dwarf galaxies ($\sim$ MeV) and galaxy clusters (~ 100 MeV). Thus the scattering process most efficient for momentum transfer is off the χ_1 particle (i.e. the "nucleus") inside H_{13}, with a cross section comparable to the H_{12} self-scattering. Therefore the geometric size of H_{13} does not lead to an enhancement, and the H_{12} isothermal profile is not significantly affected.

As structures form, the bound states fall into the overdense region and their gravitational potential energy is converted into kinetic energy, resulting in shock-heating to a temperature [53]

$$T_{gal} \approx 0.86\,\mathrm{keV}\,\frac{\mu}{10\,\mathrm{GeV}} \tag{3.19}$$

for a Milky Way sized galaxy with halo mass $10^{12} M_\odot$ and radius 110 kpc. Here μ is the total mass of all degrees of freedom that contribute to ρ_{DM} divided by their total number density, given by

$$\mu = \frac{(n_2 - n_2^f) m_{H_{12}} + (n_3 - n_3^f) m_{H_{13}} + \sum_{i=1}^{3} n_i^f m_{\chi_i}}{(n_2 - n_2^f) + (n_3 - n_3^f) + \sum_{i=1}^{3} n_i^f}. \tag{3.20}$$

If T_{gal} is higher than the binding energy, bound states can dissociate. While the more tightly bound H_{12} does not dissociate in the region of parameter space that is of interest to us, if H_{13} "reionizes" in this fashion, the scattering process $\chi_3\chi_1 \to \chi_3\chi_1\gamma_D$ can lead to efficient cooling through bremsstrahlung. For simplicity, when checking for the ionization of H_{13}, we take the initial condition to be $n_i^f = 0$. In the parameter region where H_{13} reionizes, we then recalculate T_{gal} with $n_1^f = n_3^f = n_3$ (fully reionized H_{13}) to use in the estimate for the cooling process. An estimation of the cooling time scale through this process is given by [53]

$$t_{brem} \sim 6\,\text{Gyr} \left(\frac{0.02}{\alpha_d}\right)^3 \left(\frac{0.1}{n_3/n_1}\right) \left(\frac{\mu}{10\,\text{GeV}}\right)^{\frac{1}{2}} \left(\frac{m_{H_{12}}}{10\,\text{GeV}}\right) \left(\frac{m_{\chi_3}}{1\,\text{MeV}}\right)^{\frac{3}{2}} . \tag{3.21}$$

The emitted dark photon can have a free streaming length much larger than the size of the halo, leading to halo cooling. If t_{brem} is much shorter than the age of the Milky Way (T_{MW}), a dark disc may form. Recently, results from the GAIA survey [54] have been used to set an upper bound on the fraction of the DM that can be contained in a dark disc at $\sim 1\%$ [55, 56]. A detailed study of the cooling process and the merger history of sub-halos is beyond the scope of this paper, therefore as we scan through the parameter space of our model, we will use t_{brem}/T_{MW} as a conservative indicator of whether there is a significant probability of dark disc formation. In Fig. 6, the region where H_{13} can be reionized due to shock heating is shown below the red-dotted curve, and the region where the condition for efficient bremsstrahlung cooling is satisfied is shown above the red dashed curve, resulting in the red shaded region where both conditions are satisfied and where a dark disc may form.

3.4 Reconciling the large and small scale structure problems

In figure 6, we show our combined results for several representative parameter choices, and as a function of m_{χ_3} and α_d. As mentioned in the previous section, we fix $n_2/n_1 = 0.9$. We consider 25 GeV and 45 GeV as the mass of the heaviest DM flavor, considering both possible hierarchies, $m_{\chi_1} > m_{\chi_2}$ and $m_{\chi_2} > m_{\chi_1}$.

- **Addressing the σ_8 discrepancy:** We calculate the power spectrum ratio of Eq. (3.16) for $k = 0.2h$ Mpc^{-1}, which is close to the perturbation mode for the σ_8 measurement. The contours of the power spectrum suppression depend mainly on the H_{13} recombination time scale, thus a constant power spectrum suppression traces $\alpha_d \propto (m_{\chi_3})^{-\frac{1}{2}}$ for a constant H_{13} binding energy, but they do not depend strongly on m_{χ_1}. The interesting regions for addressing the σ_8 problem are shown by the yellow bands.

- **Small scale structure:** We fix the ratio of the hyperfine splitting to the ground state energy as in Eq. (3.18). The mass of the intermediate DM flavor (χ_2 for the upper row of plots, and χ_1 for the lower row) is then determined at each point. This is indicated by the frame labels on the right-hand side of each plot. The preferred α_d interval for solving both the dwarf and cluster mass deficit problems from ref. [12] is indicated by the blue shaded bands.

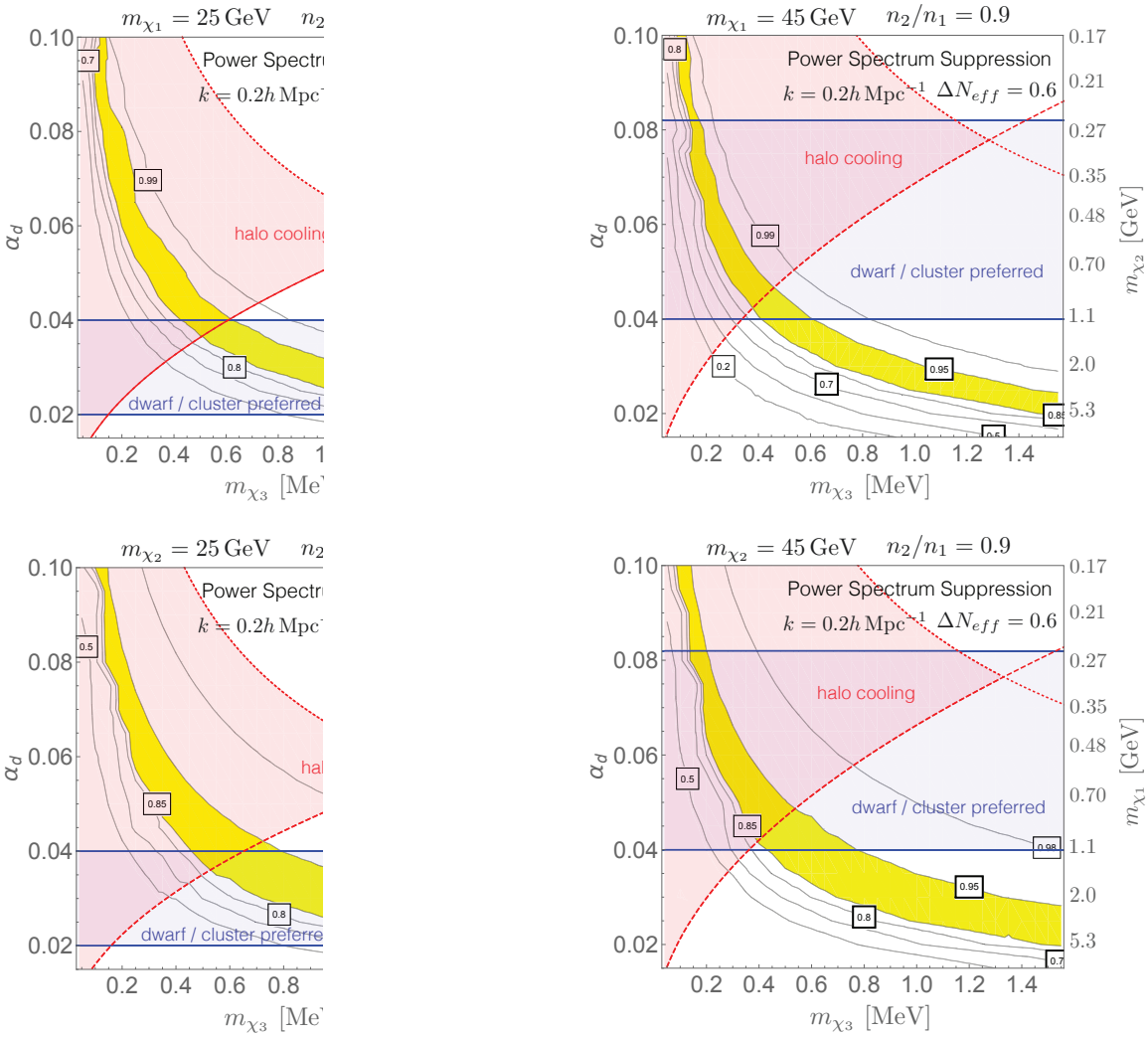

Figure 6. The combination of our results, for a few representative parameter choices. Plots on the left (right) column have the mass of the heaviest DM flavor at 25 (45) GeV. n_2/n_1 is chosen to be 0.9 in all plots. In the upper row, χ_1 is the heaviest flavor, so its mass is fixed, while the mass of χ_2 varies according to the $E_{hf}/E_0 = 10^{-4}$ benchmark we have adopted (as indicated by the frame labels on the right-hand side of the plots). In the lower row, the roles of χ_1 and χ_2 are reversed. As a function of m_{χ_3} and α_d, between the yellow shaded contours the matter power is suppressed by 5-15%, which may explain the smaller σ_8 value from late-time measurements compared to the value obtained by Planck. The blue-shaded bands show the preferred α_d interval where the mass deficit problem from dwarf galaxies to clusters is addressed. The red shaded region is disfavored by dark disc constraints as it allows for efficient cooling of the DM during halo formation. The preferred parameter space is therefore given by the overlap of the yellow and blue bands that is outside of the red shaded region.

- **Constraints from dark disc formation:** As explained in the previous section, the formation of a dark disc is possible in the red shaded region, which is therefore disfavored.

In summary, the overlap region between the yellow and blue bands that is outside of the red region gives the most preferred parameter space for addressing structure formation puzzles at different scales. This favors the ranges $\alpha_d \approx 0.02$-0.04, 20-45 GeV for the mass of the heaviest DM flavor, and the MeV scale for the mass of the lightest flavor. We reiterate that in this study we have taken a relatively simple approach to demonstrate that our model has the potential to solve the relevant structure formation problems; however a more careful study of the cosmological data and the Lyman-α constraints should be performed to fully establish this claim and determine the precise region in the parameter region where all conditions of interest are satisfied.

4 Conclusions

We have explored the cosmological and astrophysical implications of a model of Secretly Asymmetric Dark Matter, where flavor-by-flavor asymmetries are generated in the dark sector through the decay of heavy right-handed neutrinos, despite an exact gauged dark $U(1)$. As a result, the total dark charge of the universe is always zero, and the DM flavors have opposite signs of the asymmetry, making it possible for bound states to form. When the heaviest dark matter flavor has a mass of $\mathcal{O}(10)$ GeV, the intermediate flavor has a mass of $\mathcal{O}(0.1-1)$ GeV, and the lightest flavor has a mass of $\mathcal{O}(1)$ MeV, with an $\alpha_d \sim 10^{-2}$ and $n_3/n_1 \sim 0.1$, this model can address several outstanding puzzles. In particular, the dark photon as an additional degree of freedom helps resolve the discrepancy between CMB-based and low redshift measurements of H_0, the resulting dark acoustic oscillations help address the σ_8 problem, and scattering between the bound states H_{12} after halo formation, with an inelastic component through the hyperfine transition, helps resolve issues at the cluster and dwarf galaxy scales. The model is consistent with constraints from short distance physics such as bounds on millicharged DM.

We want to emphasize that while we have chosen the DM to have three flavors for simplicity, the SADM mechanism works for a larger number of flavors as well, resulting in potentially even richer dynamical phenomena due to the increased number of relevant energy scales. We leave the exploration of this possibility to future work. Note also that as experimental sensitivity to millicharged DM increases, especially as the mass threshold of direct detection experiments is lowered, the parameter region of interest to this study should become testable in the not too distant future. Also, if the mass of the mediator ϕ is smaller than the benchmark value taken in equation 2.7, the lifetime of the heavier DM flavors can enter the regime where decaying DM signatures might become observable.

Acknowledgments

The authors express special thanks to Prateek Agrawal and Siva Swaminathan for their contributions at the introductory stages of this study. We also thank Zackaria Chacko and Take Okui for helpful discussions. The research of CK and CT is supported by the National Science Foundation Grant Number PHY-1620610. YT is supported in part by the National Science Foundation Grant Number PHY-1620074 and by the Maryland Center for

Fundamental Physics (MCFP). CD is supported in part by the DOE Early Career Grant DE-SC0019225. CK and YT thank the Aspen Center for Physics, supported by National Science Foundation grant PHY-1607611, where part of this work was performed.

References

[1] P. Agrawal, C. Kilic, S. Swaminathan and C. Trendafilova, Phys. Rev. D **95**, no. 1, 015031 (2017) doi:10.1103/PhysRevD.95.015031 [arXiv:1608.04745 [hep-ph]].

[2] M. Fukugita and T. Yanagida, Phys. Lett. B **174**, 45 (1986). doi:10.1016/0370-2693(86)91126-3

[3] S. Davidson, E. Nardi and Y. Nir, Phys. Rept. **466**, 105 (2008) doi:10.1016/j.physrep.2008.06.002 [arXiv:0802.2962 [hep-ph]].

[4] C. S. Fong, E. Nardi and A. Riotto, Adv. High Energy Phys. **2012**, 158303 (2012) doi:10.1155/2012/158303 [arXiv:1301.3062 [hep-ph]].

[5] J. H. Chang, R. Essig and S. D. McDermott, JHEP **1809**, 051 (2018) doi:10.1007/JHEP09(2018)051 [arXiv:1803.00993 [hep-ph]].

[6] Z. Chacko, Y. Cui, S. Hong, T. Okui and Y. Tsai, JHEP **1612**, 108 (2016) doi:10.1007/JHEP12(2016)108 [arXiv:1609.03569 [astro-ph.CO]].

[7] M. A. Buen-Abad, M. Schmaltz, J. Lesgourgues and T. Brinckmann, JCAP **1801**, no. 01, 008 (2018) doi:10.1088/1475-7516/2018/01/008 [arXiv:1708.09406 [astro-ph.CO]].

[8] M. Raveri, W. Hu, T. Hoffman and L. T. Wang, Phys. Rev. D **96**, no. 10, 103501 (2017) doi:10.1103/PhysRevD.96.103501 [arXiv:1709.04877 [astro-ph.CO]].

[9] Z. Pan, M. Kaplinghat and L. Knox, Phys. Rev. D **97**, no. 10, 103531 (2018) doi:10.1103/PhysRevD.97.103531 [arXiv:1801.07348 [astro-ph.CO]].

[10] F. Y. Cyr-Racine and K. Sigurdson, Phys. Rev. D **87**, no. 10, 103515 (2013) doi:10.1103/PhysRevD.87.103515 [arXiv:1209.5752 [astro-ph.CO]].

[11] F. Y. Cyr-Racine, R. de Putter, A. Raccanelli and K. Sigurdson, Phys. Rev. D **89**, no. 6, 063517 (2014) doi:10.1103/PhysRevD.89.063517 [arXiv:1310.3278 [astro-ph.CO]].

[12] K. K. Boddy, M. Kaplinghat, A. Kwa and A. H. G. Peter, Phys. Rev. D **94**, no. 12, 123017 (2016) doi:10.1103/PhysRevD.94.123017 [arXiv:1609.03592 [hep-ph]].

[13] Z. Chacko, D. Curtin, M. Geller and Y. Tsai, JHEP **1809**, 163 (2018) doi:10.1007/JHEP09(2018)163 [arXiv:1803.03263 [hep-ph]].

[14] J. L. Bernal, L. Verde and A. G. Riess, JCAP **1610**, no. 10, 019 (2016) doi:10.1088/1475-7516/2016/10/019 [arXiv:1607.05617 [astro-ph.CO]].

[15] M. Persic, P. Salucci and F. Stel, Mon. Not. Roy. Astron. Soc. **281**, 27 (1996) doi:10.1093/mnras/281.1.27, 10.1093/mnras/278.1.27 [astro-ph/9506004].

[16] Hildebrandt, H., Viola, M., Heymans, C., et al. 2017, MNRAS, 465, 1454

[17] F. Köhlinger *et al.*, Mon. Not. Roy. Astron. Soc. **471**, no. 4, 4412 (2017) doi:10.1093/mnras/stx1820 [arXiv:1706.02892 [astro-ph.CO]].

[18] S. Joudaki *et al.*, Mon. Not. Roy. Astron. Soc. **474**, no. 4, 4894 (2018) doi:10.1093/mnras/stx2820 [arXiv:1707.06627 [astro-ph.CO]].

[19] M. A. Troxel *et al.* [DES Collaboration], Phys. Rev. D **98**, no. 4, 043528 (2018) doi:10.1103/PhysRevD.98.043528 [arXiv:1708.01538 [astro-ph.CO]].

[20] B. Moore, Nature **370**, 629 (1994). doi:10.1038/370629a0

[21] Newman, A. B., Treu, T., Ellis, R. S., & Sand, D. J. (2013), APJ, 765, 25

[22] J. M. Cline, Z. Liu and W. Xue, Phys. Rev. D **85**, 101302 (2012) doi:10.1103/PhysRevD.85.101302 [arXiv:1201.4858 [hep-ph]].

[23] R. Foot and S. Vagnozzi, Phys. Rev. D **91**, 023512 (2015) doi:10.1103/PhysRevD.91.023512 [arXiv:1409.7174 [hep-ph]].

[24] M. A. Buen-Abad, G. Marques-Tavares and M. Schmaltz, Phys. Rev. D **92**, no. 2, 023531 (2015) doi:10.1103/PhysRevD.92.023531 [arXiv:1505.03542 [hep-ph]].

[25] Z. Chacko, Y. Cui, S. Hong and T. Okui, Phys. Rev. D **92**, 055033 (2015) doi:10.1103/PhysRevD.92.055033 [arXiv:1505.04192 [hep-ph]].

[26] J. Lesgourgues, G. Marques-Tavares and M. Schmaltz, JCAP **1602**, no. 02, 037 (2016) doi:10.1088/1475-7516/2016/02/037 [arXiv:1507.04351 [astro-ph.CO]].

[27] P. Ko and Y. Tang, Phys. Lett. B **762**, 462 (2016) doi:10.1016/j.physletb.2016.10.001 [arXiv:1608.01083 [hep-ph]].

[28] P. Ko and Y. Tang, Phys. Lett. B **768**, 12 (2017) doi:10.1016/j.physletb.2017.02.033 [arXiv:1609.02307 [hep-ph]].

[29] V. Prilepina and Y. Tsai, JHEP **1709**, 033 (2017) doi:10.1007/JHEP09(2017)033 [arXiv:1611.05879 [hep-ph]].

[30] P. Agrawal, F. Y. Cyr-Racine, L. Randall and J. Scholtz, JCAP **1708**, no. 08, 021 (2017) doi:10.1088/1475-7516/2017/08/021 [arXiv:1702.05482 [astro-ph.CO]].

[31] I. Baldes, M. Cirelli, P. Panci, K. Petraki, F. Sala and M. Taoso, SciPost Phys. **4**, no. 6, 041 (2018) doi:10.21468/SciPostPhys.4.6.041 [arXiv:1712.07489 [hep-ph]].

[32] J. March-Russell, C. McCabe and M. McCullough, JHEP **1003**, 108 (2010) doi:10.1007/JHEP03(2010)108 [arXiv:0911.4489 [hep-ph]].

[33] B. Batell, J. Pradler and M. Spannowsky, JHEP **1108**, 038 (2011) doi:10.1007/JHEP08(2011)038 [arXiv:1105.1781 [hep-ph]].

[34] P. Agrawal, S. Blanchet, Z. Chacko and C. Kilic, Phys. Rev. D **86**, 055002 (2012) doi:10.1103/PhysRevD.86.055002 [arXiv:1109.3516 [hep-ph]].

[35] J. Kile, Mod. Phys. Lett. A **28**, 1330031 (2013) doi:10.1142/S0217732313300310 [arXiv:1308.0584 [hep-ph]].

[36] P. Agrawal, M. Blanke and K. Gemmler, JHEP **1410**, 072 (2014) doi:10.1007/JHEP10(2014)072 [arXiv:1405.6709 [hep-ph]].

[37] M. C. Chen, J. Huang and V. Takhistov, JHEP **1602**, 060 (2016) doi:10.1007/JHEP02(2016)060 [arXiv:1510.04694 [hep-ph]].

[38] P. Agrawal, Z. Chacko, E. C. F. S. Fortes and C. Kilic, Phys. Rev. D **93**, no. 10, 103510 (2016) doi:10.1103/PhysRevD.93.103510 [arXiv:1511.06293 [hep-ph]].

[39] Goldberg, H., & Hall, L. J. 1986, Physics Letters B, 174, 151

[40] D. E. Kaplan, G. Z. Krnjaic, K. R. Rehermann and C. M. Wells, JCAP **1005**, 021 (2010) doi:10.1088/1475-7516/2010/05/021 [arXiv:0909.0753 [hep-ph]].

[41] N. Aghanim *et al.* [Planck Collaboration], arXiv:1807.06209 [astro-ph.CO].

[42] A. G. Riess *et al.*, Astrophys. J. **861**, no. 2, 126 (2018) doi:10.3847/1538-4357/aac82e [arXiv:1804.10655 [astro-ph.CO]].

[43] V. Bonvin *et al.*, Mon. Not. Roy. Astron. Soc. **465**, no. 4, 4914 (2017) doi:10.1093/mnras/stw3006 [arXiv:1607.01790 [astro-ph.CO]].

[44] K. Kadota, T. Sekiguchi and H. Tashiro, arXiv:1602.04009 [astro-ph.CO].

[45] A. G. Riess *et al.*, Astrophys. J. **826**, no. 1, 56 (2016) doi:10.3847/0004-637X/826/1/56 [arXiv:1604.01424 [astro-ph.CO]].

[46] Riess, A. G., Casertano, S., Yuan, W., et al. 2018, APJ, 855, 136

[47] R. Cooke, M. Pettini, R. A. Jorgenson, M. T. Murphy and C. C. Steidel, Astrophys. J. **781**, no. 1, 31 (2014) doi:10.1088/0004-637X/781/1/31 [arXiv:1308.3240 [astro-ph.CO]].

[48] J. M. Cline, Z. Liu, G. Moore and W. Xue, Phys. Rev. D **89**, no. 4, 043514 (2014) doi:10.1103/PhysRevD.89.043514 [arXiv:1311.6468 [hep-ph]].

[49] C. P. Ma and E. Bertschinger, Astrophys. J. **455**, 7 (1995) doi:10.1086/176550 [astro-ph/9506072].

[50] R. Krall, F. Y. Cyr-Racine and C. Dvorkin, JCAP **1709**, no. 09, 003 (2017) doi:10.1088/1475-7516/2017/09/003 [arXiv:1705.08894 [astro-ph.CO]].

[51] M. Garny, T. Konstandin, L. Sagunski and S. Tulin, JCAP **1809**, no. 09, 011 (2018) doi:10.1088/1475-7516/2018/09/011 [arXiv:1805.12203 [astro-ph.CO]].

[52] A. D. Rivero, C. Dvorkin, F. Y. Cyr-Racine, J. Zavala and M. Vogelsberger, arXiv:1809.00004 [astro-ph.CO].

[53] J. Fan, A. Katz, L. Randall and M. Reece, Phys. Dark Univ. **2**, 139 (2013) doi:10.1016/j.dark.2013.07.001 [arXiv:1303.1521 [astro-ph.CO]].

[54] Gaia Collaboration, Prusti, T., de Bruijne, J. H. J., et al. (2016), A&A, 595, A1

[55] K. Schutz, T. Lin, B. R. Safdi and C. L. Wu, Phys. Rev. Lett. **121**, no. 8, 081101 (2018) doi:10.1103/PhysRevLett.121.081101 [arXiv:1711.03103 [astro-ph.GA]].

[56] J. Buch, J. S. C. Leung and J. Fan, arXiv:1808.05603 [astro-ph.GA].